SANDIA REPORT
SAND2013-5247
Unlimited Release
Printed July 2013

Characterization of X-Ray Generator Beam Profiles

Dean J. Mitchell, Kyle Thompson, Lee T. Harding, Gregory G. Thoreson,
Lisa Theisen, and John E. Parmeter

Prepared by
Sandia National Laboratories
Albuquerque, New Mexico 87185 and Livermore, California 94550

Sandia National Laboratories is a multi-program laboratory managed and operated by Sandia Corporation, a wholly owned subsidiary of Lockheed Martin Corporation, for the U.S. Department of Energy's National Nuclear Security Administration under contract DE-AC04-94AL85000.

Issued by Sandia National Laboratories, operated for the United States Department of Energy by Sandia Corporation.

Available to DOE and DOE contractors from

U.S. Department of Energy
Office of Scientific and Technical Information
P.O. Box 62
Oak Ridge, TN 37831

Telephone: (865) 576-8401
Facsimile: (865) 576-5728
E-Mail: reports@adonis.osti.gov
Online ordering: http://www.osti.gov/bridge

Available to the public from

U.S. Department of Commerce
National Technical Information Service
5285 Port Royal Rd.
Springfield, VA 22161

Telephone: (800) 553-6847
Facsimile: (703) 605-6900
E-Mail: orders@ntis.fedworld.gov
Online order: http://www.ntis.gov/help/ordermethods.asp?loc=7-4-0#online

SAND2013-5247

Printed July 2013

Characterization of X-Ray Generator Beam Profiles

Dean J. Mitchell, Lee T. Harding, Gregory G. Thoreson,
Lisa Theisen, and John Parmeter
Contraband Detection

Kyle Thompson
Experimental Mechanics/NDE & Model Validation

Sandia National Laboratories
P.O. Box 5800
Albuquerque, NM 87185-0782

Abstract

T to compute the radiography properties of various materials, the flux profiles of X-ray sources must be characterized. This report describes the characterization of X-ray beam profiles from a Kimtron industrial 450 kVp radiography system with a Comet MXC-45 HP/11 bipolar oil-cooled X-ray tube. The empirical method described here uses a detector response function to derive photon flux profiles based on data collected with a small cadmium telluride detector. The flux profiles are then reduced to a simple parametric form that enables computation of beam profiles for arbitrary accelerator energies.

Contents

Figures

Tables

Acronyms

GADRAS Gamma Detector Response and Analysis Software

Executive Summary

This report describes characterization of beam profiles for common x-ray generators, which produce x-rays by accelerating electrons into tungsten targets. The resulting Bremsstrahlung radiation yields a continuous distribution of photons with an end point defined by the accelerator voltage. The x-ray generation system that was characterized was a Kimtron industrial 450 kVp system with a Comet MXC-451HP/11 bipolar oil-cooled X-ray tube.

The long-term objective of this work is to enable accurate computations of material X-ray attenuation properties and radiographs based on three-dimensional descriptions of inspected items. A method that is often used to simulate radiographs is to compute simple transmission profiles, and the simulations often approximate x-ray beams as if they were monoenergetic. The resulting simulations produce images that generally contain much more detail than as-measured radiographs. More realistic simulations require an accurate description of beam profile as well as a sensitivity profile for the radiographic film or plate. It was somewhat surprising when we began this work to find that x-ray beam profiles are not generally available for common, commercially available X-ray generators. Although Monte Carlo codes have been used to estimate beam profiles, measured spectra are not available to validate the accuracy of the calculations. The empirical method that is described in this report uses a detector response function to derive photon flux profiles based on measurements collected by a small CdTe detector. The flux profiles are then reduced to a simple parametric form that enables computation of beam profiles for arbitrary accelerator energies.

1 Introduction

There is currently much interest within the homeland security and defense communities in improvised or homemade explosives (HME). The radiographic properties of HMEs are of particular interest since it is possible that these properties can be used in some circumstances to distinguish HME materials from innocuous materials. Towards this end, a Laboratory Directed Research and Development (LDRD) project is underway to attempt to measure the x-ray attenuation properties of HME, and to calculate them theoretically. A necessary first step for the experimental measurements is the detailed characterization of the x-ray spectrum of the x-ray source to be used in the measurements. Common commercial sources generally produce Bremsstrahlung radiation, with the resulting X-rays having a large range of energies. This produces a situation that is much more complex than if a monoenergetic x-ray source were used, and source characterization is therefore critical. This report describes in detail the source characterization for an experimental system currently is use at Sandia National Laboratories.

The principal challenge that was encountered during this investigation was accommodation of the large dynamic range separating the photon flux for sealed gamma-ray calibration sources and the much greater flux associated with x-ray generators. In order to avoid excessive random pulse pileup, measurements of the x-ray beam were performed with a small (0.3cm×0.3cm×0.1cm) CdTe detector at the largest distance that could be accommodated in the measurement facility (384 cm from the radiography source). Even under these conditions, the count rate would have been excessive if measurements were to have been performed with the bare detector, so copper (Cu) and tin (Sn) filters were used to attenuate low-energy photons. In contrast to the radiography beam measurements, characterization measurements were performed at a distance of only 20 cm, and long measurement times were required to obtain data with acceptable statistical confidence.

2 Theory

The Gamma Detector Response and Analysis Software (GADRAS)[1] was used to characterize the CdTe detector response. The GADRAS application computes the response based on known interaction cross sections for the detector material. Empirical parameters are applied to characterize detector-specific features, such as energy calibration, resolution, and the incidence of scattered radiation. GADRAS also contains a collection of regression algorithms, which were applied to compute flux profiles that reproduce the spectra.

The objective of this investigation is to develop a general method for computing beam profiles that is flexible enough to describe the output under conditions that were not measured explicitly during this investigation. Hence, the results of all of the measurements were used to derive a simple, analytic description of the beam profile as a continuous function of the accelerator voltage. Adjustment of the beam profile associated with the use of filter materials was also investigated. The computational consistency was then validated by comparing measured spectra with calculations based on the analytic description of the beam profile.

3 Experimental Procedure

Two types of x-ray output measurements were performed using an industrial x-ray system, output dose rate and output beam spectrum. The equipment used for these measurements is shown in Table 1.

Table 1 Experimental Equipment

Component	Description
X-ray System	Kimtron 450 kV industrial x-ray system
X-ray Tube	Comet MXR-451HP/11
Dose Rate Detector	Radcal 9010 with a 0.6 cc ion chamber
X-ray Spectrum Detector	Amptek PX4 Digital Pulse Processor and a XR-100T CdTe (0.3x0.3x0.1mm CdTe element) X-ray Detector
Filter materials	0.2 cm Cu and 0.075 cm Sn sheets

3.1 X-ray Dose Rate Measurements

X-ray dose measurements were conducted using a Radcal 9010 detector with a 0.6 cc ion chamber. The x-ray system/tube output beam profile was measured by positioning the 0.6 cc ion chamber 1 meter from the focal spot of the x-ray tube. The x-ray tube was positioned with the tube axis horizontal. Measurements were taken directly in front of the x-ray tube and at angular offsets with 5 degree increments both horizontally and vertically. The x-ray tube voltage was varied from 50 kVp to 450 kVp in steps of 50 kV with a tube current of 1 mA and the large focal spot.

Additional output dose measurements were performed to measure the relationship between tube current and x-ray output. For these measurements, the Radcal 0.6 cc ion chamber was positioned directly in front of the x-ray tube, 1 meter from the x-ray tube focal spot. The x-ray tube voltage was varied from 50 kVp to 450 kVp in steps of 50 kV. The x-ray tube current was varied from 0.1 mA to a maximum of 10 mA (Note: If the x-ray system was not able to operate at 10 mA for the kVp selected, the maximum operating value was used) and the large focal spot was used.

X-ray dose measurements were also acquired while the beam spectrum was being measured. For these measurements, the 0.6 cc ion chamber was positioned 26 cm from the x-ray focal spot and slightly off the perpendicular axis of the tube beam port. This allowed for an unimpeded path from the x-ray tube to the spectrum measurement detector.

3.2 X-ray Spectrum Measurements

An Amptek CdTe detector was used to measure the x-ray beam spectrum. The Amptek detector was positioned 384 cm from the x-ray tube focal spot. The Amptek detector settings are listed in Table 2.

Table 2 Amptek Detector Settings

Setting	Value
Gain	4.95
Acquisition time	120 seconds
HV voltage	498 V
Dead time	< 10%
MCA Channels	4096

Spectrum measurements were recorded with x-ray tube voltages from 50 kVp to 150 kVp, x-ray tube current of 0.1 mA, and a 0.2 cm copper filter directly in front of the detector. Additional spectrum measurements were taken with x-ray tube voltages from 100 kVp to 450 kVp, x-ray tube current of 0.1 mA, and a 0.15 cm tin filter directly in front of the detector.

The lowest x-ray tube current was used to avoid saturating the detector and maintain a detector dead time below 10%.

Figure 1 shows the setup of the Kimtron 450 kV system. Figures 2 and 3 show the detector setup for the copper filter and tin filter configurations.

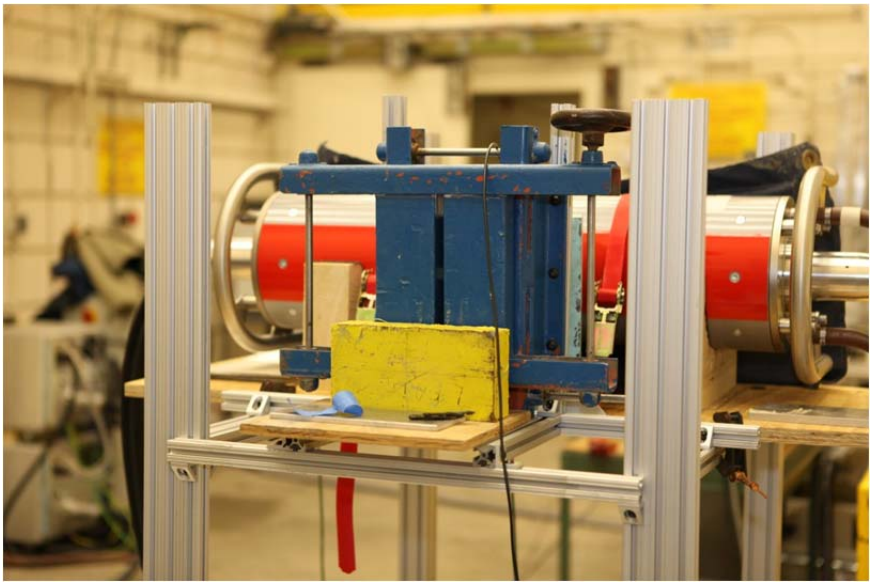

Figure 1 Kimtron 450 kV industrial x-ray system.

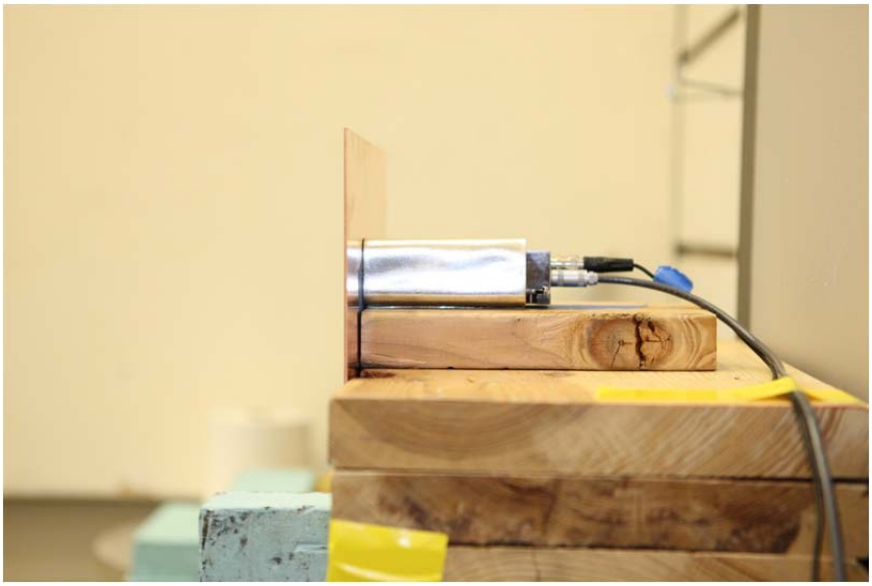

Figure 2 Amptek CdTe detector behind 0.2 cm thick copper sheet.

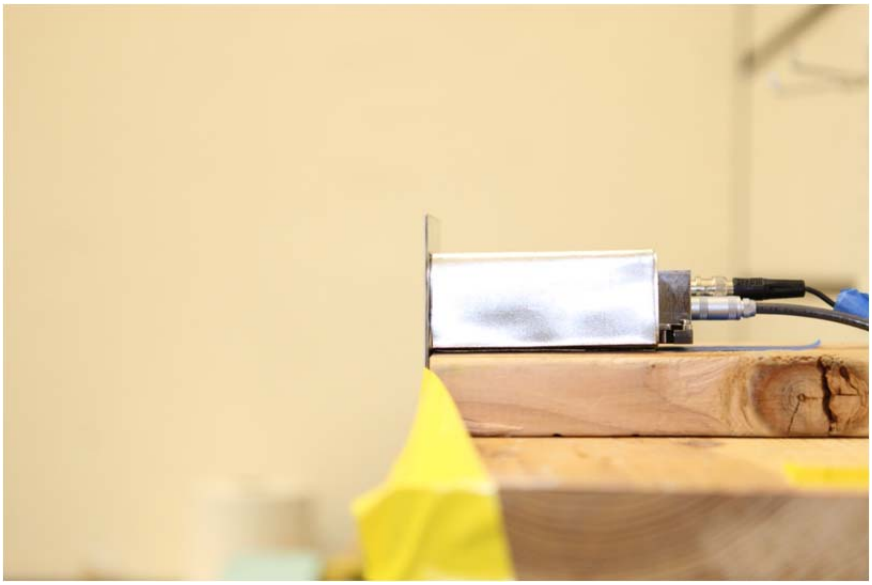

Figure 3 Amptek CdTe detector behind 0.15 cm thick tin sheet

4 Results

4.1 X-ray Tube Characterization

Measurements were performed to determine the x-ray tube output variation as a function of position and tube current for a Kimtron 450 kV industrial x-ray system with a Comet MXR-451HP/11 x-ray tube.

4.1.1 X-ray Tube Output vs position

The output (dose rate) of the x-ray tube was measured using a Radcal 9010 detector with a 0.6 cc ion chamber. The detector was positioned 1 meter from the x-ray tube focal spot and moved in 5 degree increments horizontally and vertically from a position perpendicular to the tube face. The output is normalized to a position 1 meter in front of the x-ray tube. Negative horizontal positions are closer to the negative high voltage input cable. Figure 4 shows the relative horizontal variation in the x-ray tube output. Figure 5 shows the relative vertical variation in the x-ray tube output.

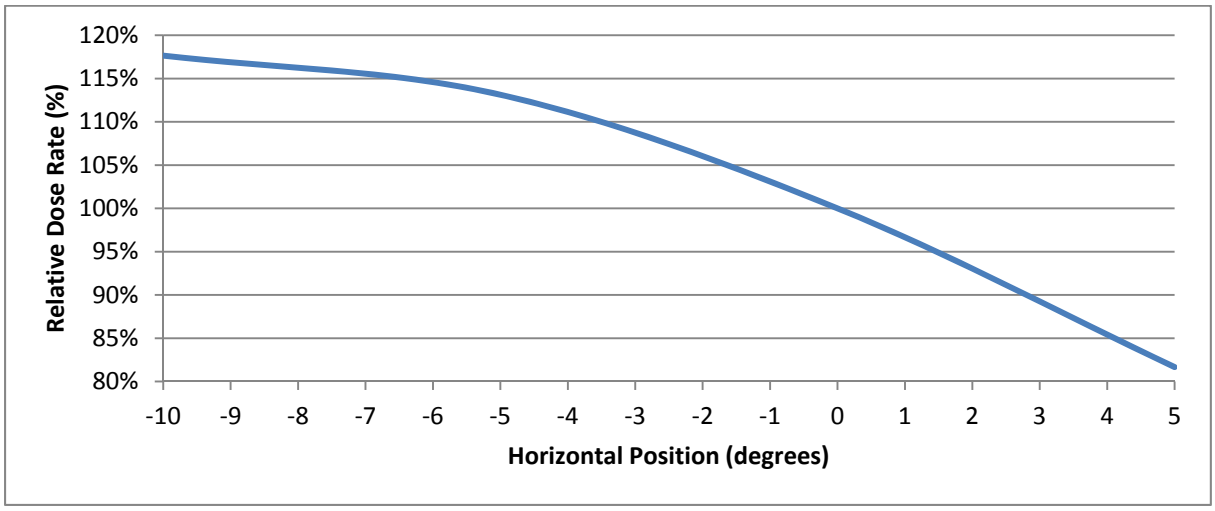

Figure 4 Relative X-ray tube output vs. horizontal position.

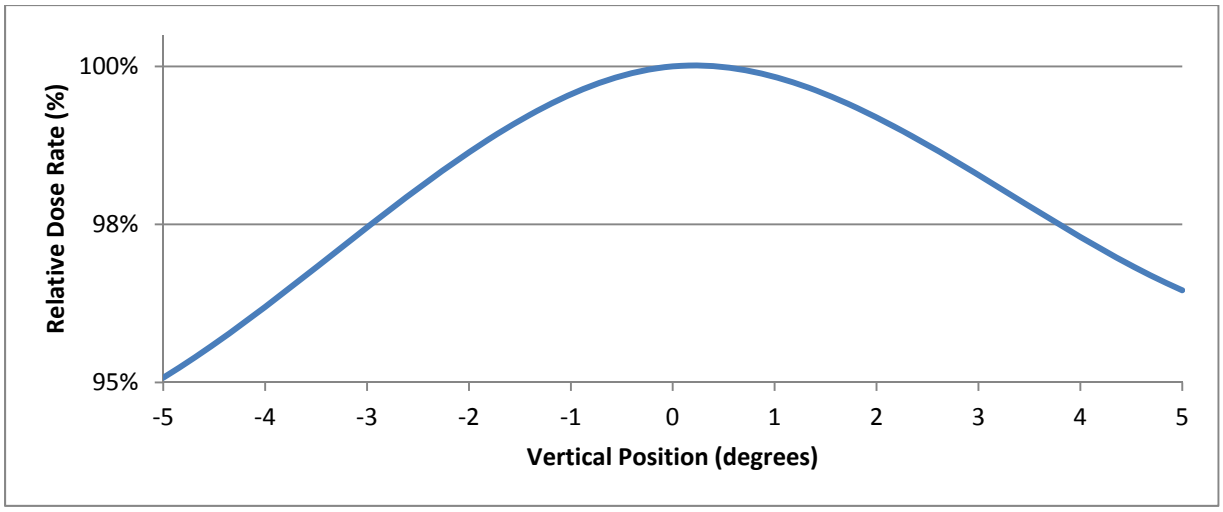

Figure 5 Relative X-ray tube output vs.vertical position.

4.1.2 X-ray Tube Output vs Current

The output (dose rate) of the x-ray tube was measured using a Radcal 9010 detector with a 0.6 cc ion chamber for various peak voltage and current settings. The detector was positioned 1 meter from the x-ray tube focal spot at a position perpendicular to the tube face. Figure 6 shows the measured values in R/hr/mA for peak x-ray voltages ranging from 50 kV to 450 kV.

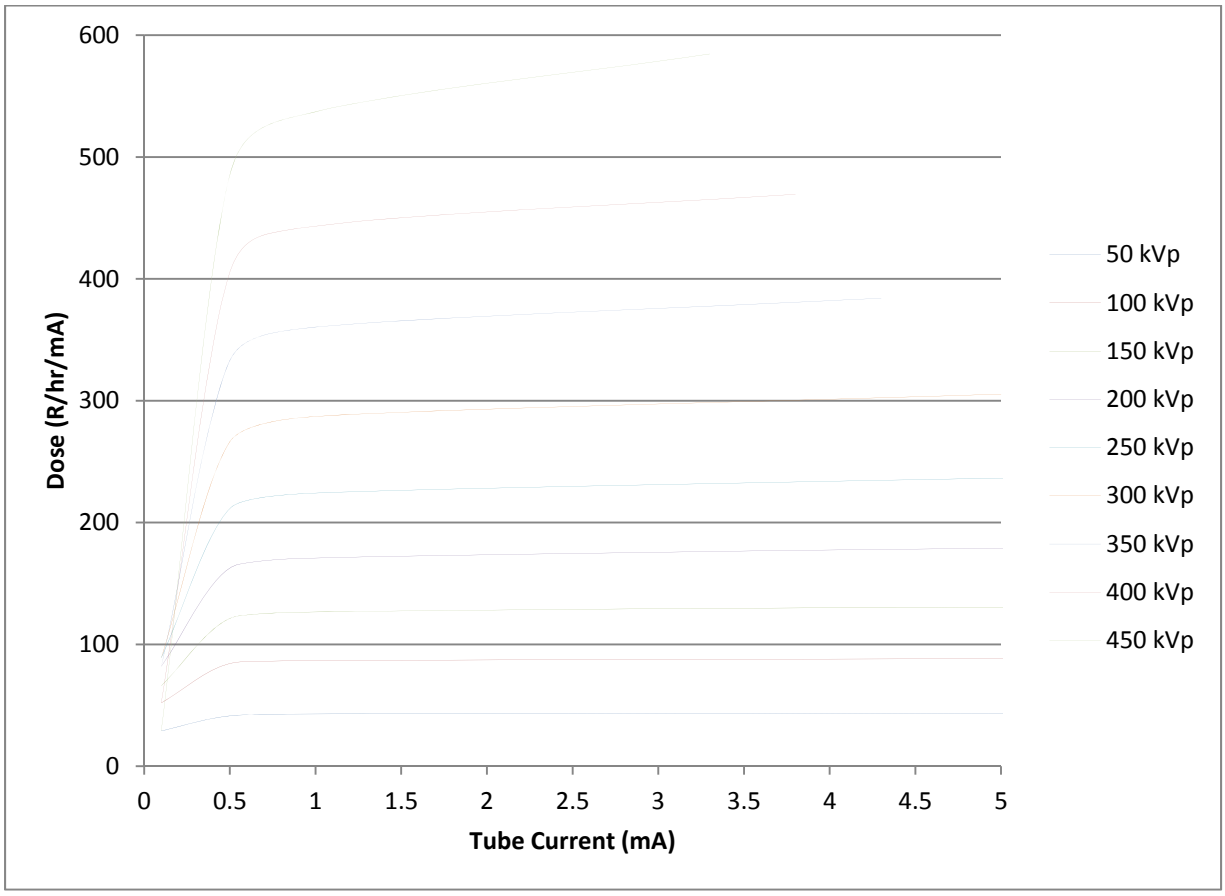

Figure 6 Measured X-ray Tube Output as a function of tube current.

Figure 6 indicates that the x-ray system output is approximately proportional to the tube current above 0.5 mA. When the system is operated at 0.1 mA (the lowest setting for the device), the output deviates significantly.

4.2 Detector Characterization

Characterization measurements were performed by measuring a series of nominal 100 µCi calibration sources at a distance of 20 cm from the surface of the CdTe detector. Measurements were performed for the following configurations:

- Bare detector
- Detector behind a 0.20 cm thick copper filter
- Detector behind a 0.15 cm thick tin filter

Measurements that were recorded when the detector was behind the copper and tin filters are relevant because filters were required to avoid excessive random pulse pileup when measurements of the x-ray generator were recorded. The use of filters of various types is also a common practice that is applied to tailor photon flux profiles to optimize contrast in radiographs. Therefore, evaluation of the ability to compute flux profiles when filters are present is an essential aspect of this investigation.

Figure 7 is a plot of the photopeak efficiency and the Compton efficiencies that are calculated by GADRAS. Figure 8 compares computed spectra with measurements that were recorded when the bare detector was exposed to ^{133}Ba and ^{137}Cs sources. The best fit to the data was obtained when the detector length was defined as 0.08 cm whereas the manufacturer's specification lists the thickness as 0.010 cm. This difference is likely associated with incomplete charge collection in the dead layers near the electrical contacts. Other parameters in the response function describe the resolution and peak shape. The photopeaks in measured data exhibit more pronounced low-energy tails for high-energy photons relative to computed spectra based on the response function, which is optimized for considerably larger detectors. However, the principal objective is to characterize the Bremsstrahlung continuum, so the accuracy of the peak shapes does not impact the results appreciably. Therefore, the parameters that describe the detector thickness and dead layers were adjusted empirically to fit peak areas, which are more important than peak shapes. The peak areas are reproduced to within 10% over the energy range 60 keV to 661 keV. Computed continua derived from Compton scattering interaction agree well with measurements without adjustment. The detector response was also characterized when the detector was placed behind the copper and tin filters, so that effects associated with attenuation and scattering produced by the filters are incorporated into the detector response. The accuracy of characterizations that were obtained when filters were inserted was similar to results that were obtained for the bare detector.

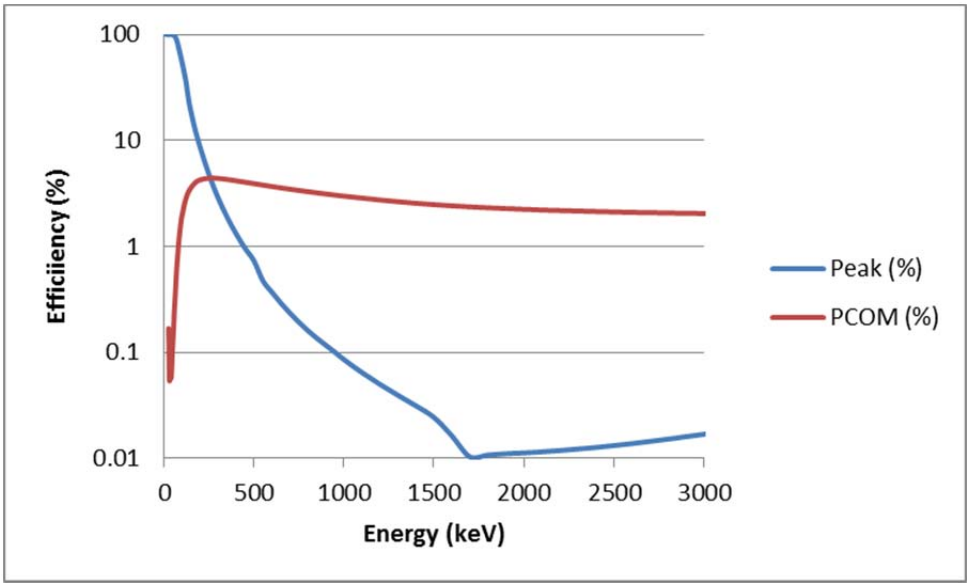

Figure 7 Detector Photopeak and Compton efficiencies.

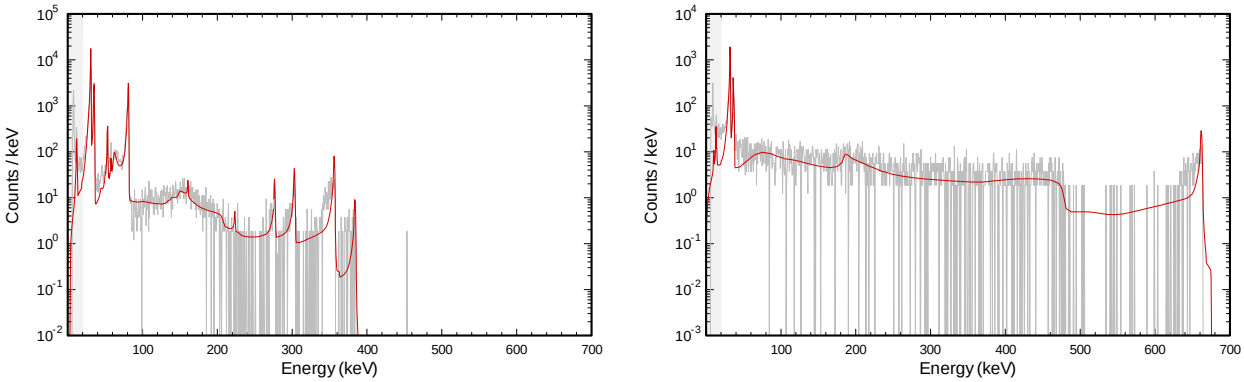

Figure 8 Comparison of measured (gray) for the bare CdTe detector and computed spectra (red) for ^{133}Ba and ^{137}Cs sources at a distance of 20 cm.

4.3 Flux Calculations

All of the measurements described in this section were obtained with the x-ray generator current set at 0.1 mA, which is the lowest current obtainable with this equipment. Spectral shapes that were observed for higher currents were consistent with the 0.1 mA spectra, but a rigorous evaluation could not be performed because random pulse pileup compromised the value of data for substantially higher currents.

Photon flux profiles were evaluated using multiple linear regression to fit measured spectra with a combination of computed spectral templates. The following process was applied:

- Spectra were inspected to identify photopeaks.
- Templates were computed for discrete gamma rays with energies corresponding to the identified peaks.
- A continuum energy-group structure was defined that extended to the electron beam energy.
- Templates were computed for each of the continuum energy groups, where it was assumed that the relative flux was constant within each of the energy groups.
- A calculation was performed to estimate the portion of the measured spectrum that was derived from random pulse pileup. The estimated pileup spectrum was used to correct the measured spectrum to remove pileup effects as much as possible.
- Multiple linear regression was used to fit the pileup-corrected, measured spectrum with a combination of spectral templates that minimized the χ^2 difference between the measured and computed spectra.

Figure 9 presents a graphic example of the result that was obtained by analyzing the spectrum for the x-ray generator at a voltage of 120 keV with the 0.20 cm thick copper filter placed in front of the detector. Photopeaks that were identified in the 60 keV region correspond to x-rays that were emitted by the tungsten converter in the x-ray generator. The estimated continuum, which extends to the energy of the electron beam, exhibits little structure other than what can be

attributed to artifacts associated with the fitting procedure. No attempt is made to fit the spectrum below about 35 keV because, as a result of attenuation imposed by the copper filter, the majority of counts in this region are derived from scattered radiation. The fitting procedure does not use peak terms below the 35keV cutoff, so photopeaks below 35 keV in Figure 9 are derived with the escape of fluorescence x-rays from the CdTe as opposed to discrete gamma rays striking the surface of the detector. The low-energy cutoff increases to about 60 keV for measurements that were performed with the tin filter due to the higher absorption coefficient of tin.

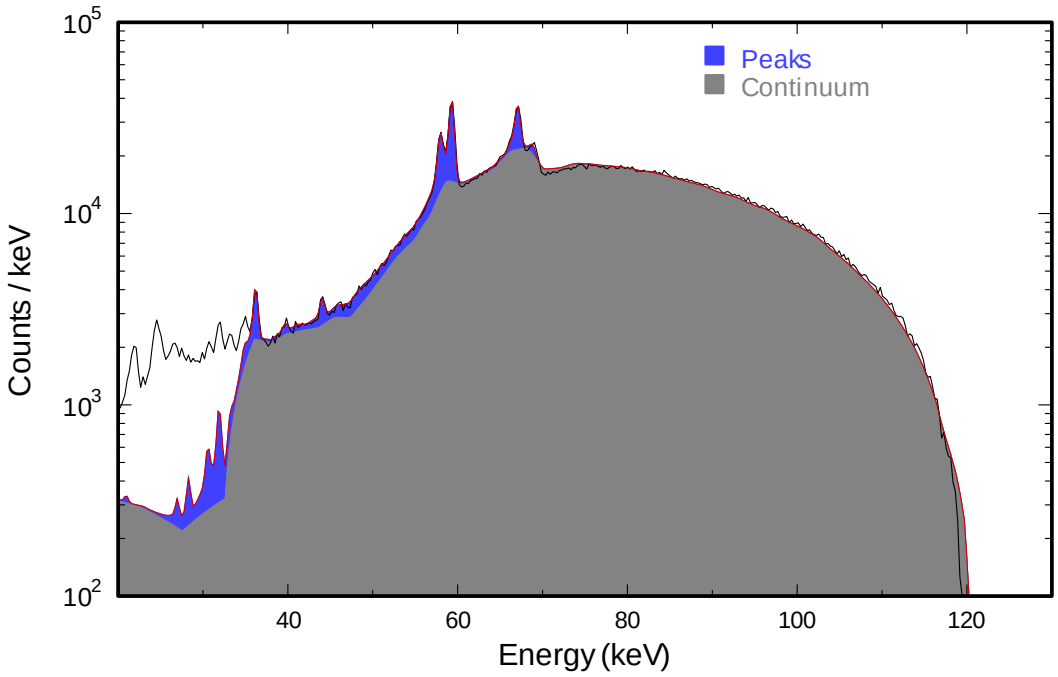

Figure 9. Comparison of measured (black line) and computed spectrum for the x-ray generator at an electron voltage of 120 keV. The gray filled region corresponds to the Bremsstrahlung continuum and the blue filled region corresponds to the component of the spectrum associated with photopeaks.

Figure 10 presents continuum flux profiles that were obtained by analyzing measurements that were collected while the tin filter was in place. A comparable series of flux profiles was generated for the copper filter, but the maximum accelerator energy for these measurements was 150 keV because excessive random pulse pileup was encountered at higher energies. Measurements at 100 keV, 120 keV, and 150 keV were repeated using both copper and tin filters as a means of evaluating systematic errors. The computed flux profiles were consistent for these overlapping measurements except below 60 keV, where the tin filter eliminated most of the direct radiation, and in the high-energy regions, where random pulse pileup compromised results derived from measurements with the copper-filter.

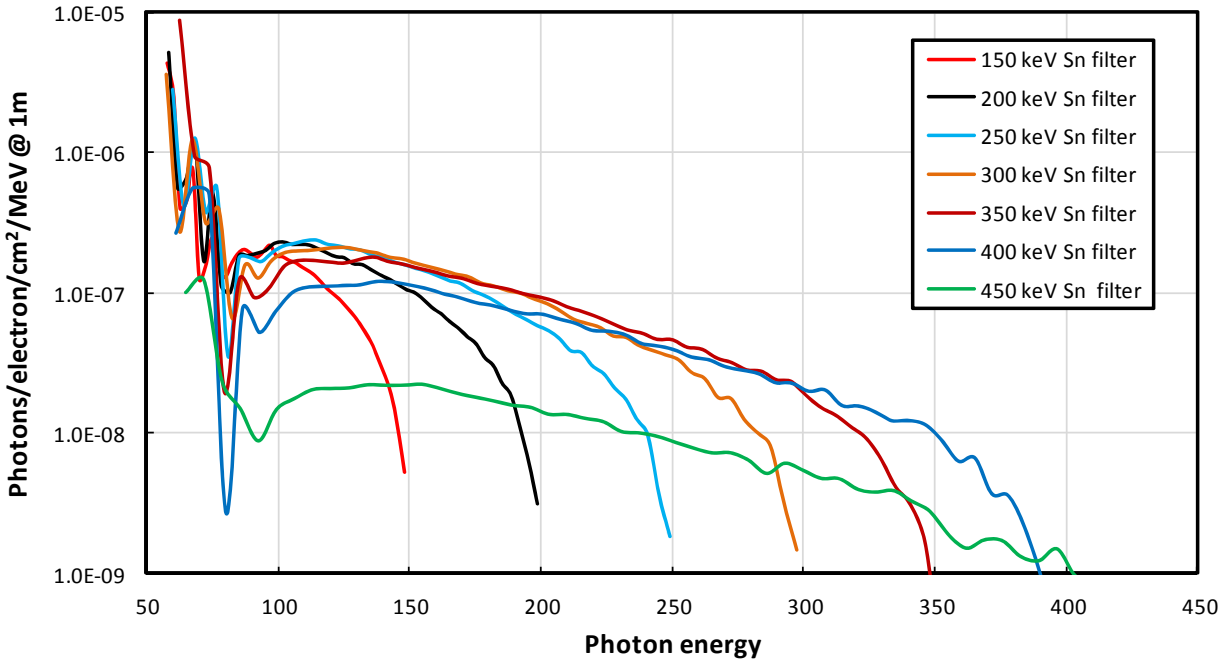

Figure 10. Computed photon profiles derived from measurements with the tin filter.

4.4 Analytic Representation of Flux Profiles

Flux profiles presented in
Figure 10 could be interpolated to derive profiles at intermediate energies. However, utilization of an analytic representation versus interpolation of tabulated values is preferable because of computational efficiency, and development of an analytic model can also eliminate some of the computational artifacts. Experimentation with a few methods of reducing the data revealed a simple method for consolidating all of the data. As shown in Figure 11, a simple transformation of the horizontal axis presents the data in a form where each of the flux profiles can be fit with the simple, two-parameter power relationship shown in Equation (1).

$$F_\gamma = s\left[1 - \left(\frac{E_\gamma}{E_e}\right)\right]^p \tag{1}$$

The parameter E_γ is the photon energy; E_e is the electron energy; s and p are the two adjustable parameters represented by the trend lines in Fig. 11. The flux at photon energy E_γ, which is represented as F_{γ_2} is expressed according to the common convention using units of photon/electron/cm^2/MeV at a distance of 1 meter.

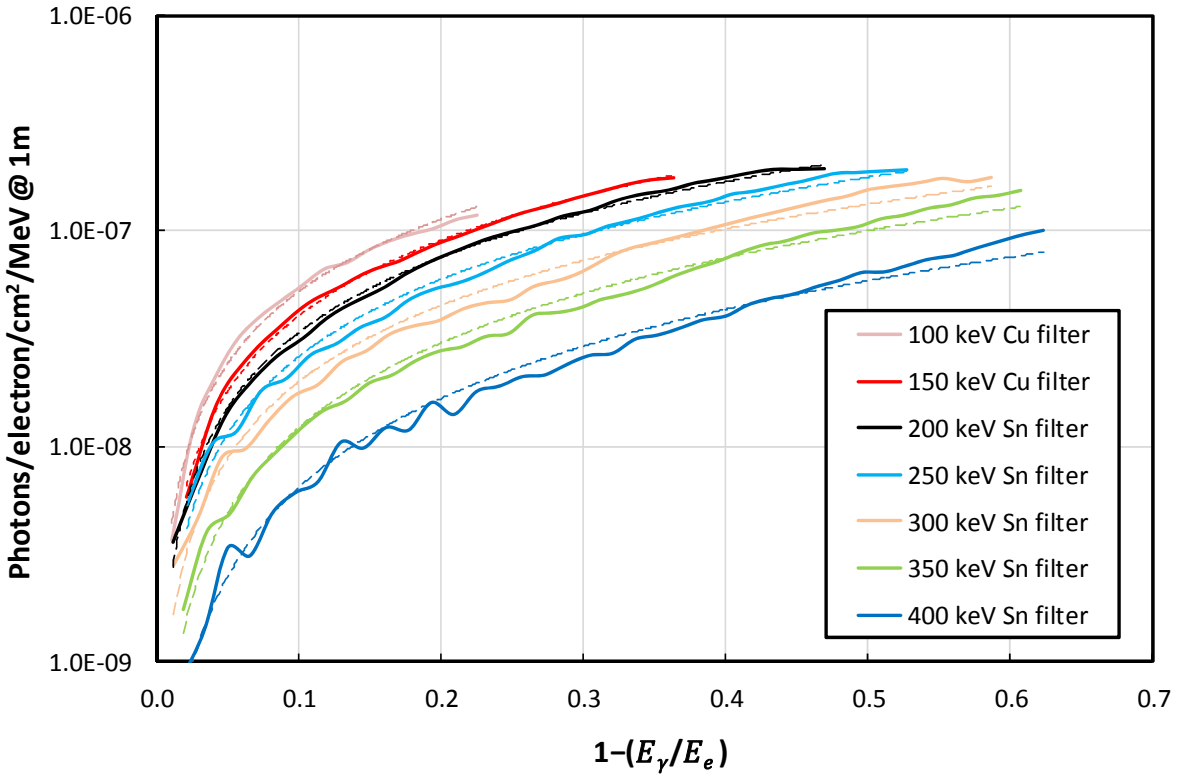

Figure 11. Following a simple transformation of the horizontal axis, computed photon profiles (solid lines) can be fit with reasonable accuracy by two-parameter power relationships illustrated by the dotted curves.

Figure 11 does not include low-energy data (i.e., large abscissa values) because scattered radiation dominates the detector response below a cutoff energy imposed by the radiography filter. Consequently, the flux of low-energy photons is determined more accurately based on measurements with the copper filter relative to data that were acquired with the tin filter. Accordingly, Figure 11 shows measurements with the copper filter for electron voltages of 100 keV and 150 keV; the tin filter is required for higher energies because random pulse pileup would be excessive otherwise.

The two adjustable parameters, s and p, in Equation (1) vary systematically with the accelerator voltage. The values of these parameters can be computed according to Equations (2) and (3) as a function of the accelerator voltage, E_e, which is given in units of MeV. Therefore, the Bremsstrahlung continuum emitted by the x-ray generator can be determined as a function of the accelerator voltage using only Equations (1-3) without reference to any look-up tables.

$$s = (0.80 - 1.63 \times E_e) \times 10^{-6} \tag{2}$$

$$p = 1.0204 + 0.7738 \times E_e \tag{3}$$

4.5 Tungsten X-Ray Yields

Radiographic images that are produced by low-energy x-ray generators may be strongly influenced by tungsten x-rays, which are emitted when the electron beam strikes the tungsten converter. The tungsten x-rays can represent a substantial portion of the total photon emission. The flux rate of tungsten x-rays (photons/cm^2/electron at 1 m) can be expressed according to the following relationship:

$$F_{x_i} = F_\gamma\big|_{70\ keV} Y_{x_i}[80 \times (E_e - 0.05)] \tag{4}$$

where $F_\gamma\big|_{70\ keV}$ is the continuum photon flux at 70 keV and $Y_{x_i}$is the relative x-ray yield. The energies and relative yields of tungsten x-rays are listed in Table 3. This relationship is based on the continuum flux at 70 keV because lower-energy x-rays do not have sufficient energy to dislodge K-shell electrons in tungsten, which must occur to produce the x-rays.

Table 3. Relative yields of tungsten x-rays.

X-ray Energy (keV)	Relative yield
57.98	0.288
59.32	0.500
67.20	0.169
69.10	0.043

4.6 Radiography Filters

The copper filter that is referenced in this paper is the standard filter that is used in association with the x-ray generator. Other filter materials, such as tin, can be used to adjust the x-ray profile. The method that is used to compute the resulting beam profile must be sufficiently flexible to accommodate a variety of material compositions and thicknesses. The principal effect of filters is to preferentially absorb low-energy photons, but filters also down-scatter radiation to low energy. The GADRAS application contains a subroutine that computes scattering as well as attenuation, and this subroutine is applied to determine the flux profile for arbitrary filter materials.

4.7 Forward Calculations

Several approximations were made in order to reduce measured data into a form that permits computation of beam profiles based on Equations (1-4). The applicability of this approach can be evaluated by performing forward calculations, where the estimated beam profiles are combined with the detector response function to compute spectra. Forward calculations that are presented in this section are based on the response function for the bare CdTe detector, and the flux is adjusted based the atomic number and areal density that is specified for radiography filters if they are used. Although the distinction is subtle, it should be noted that the flux profiles were derived from response function parameters that include the filter materials as part of the detector response characteristics, whereas calculations presented in this section apply the response function parameters for the bare detector to flux profiles that have been adjusted for effects associated with the radiography filters.

Figure 12 compares calculations with measured spectra that were recorded at an accelerator voltage of 100 keV. The computed spectra are in reasonably good agreement with measurements that were recorded with both copper and tin filters. As noted previously, measurements that are recorded with the copper filter are influenced by random pulse pileup, which occurs when two photons strike the detector close enough in time such that they cannot be resolved. The resulting pulse corresponds to an energy that exceeds either of the individual photons. Accordingly, the continua above 100 keV are produced by random pileup. Figure 13 compares measured and computed spectra that were recorded at an accelerator voltage of 150 keV. Count rates were excessive using the copper filter for accelerator voltages exceeding 150 keV, so the tin filter was used for all measurements at higher energies. Figure 14 compares measured and computed spectra over the range 200 keV to 400 keV.

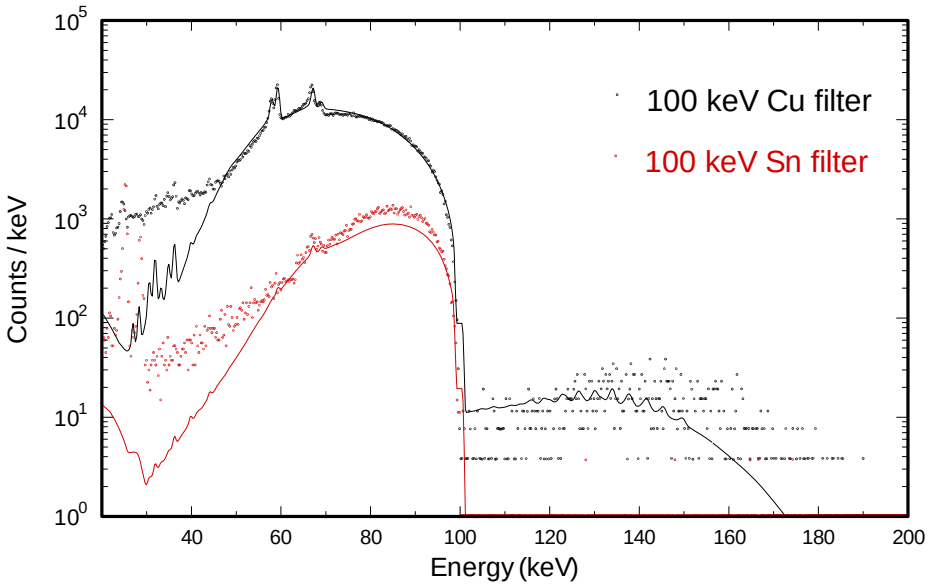

Figure 12. Computed spectra at an x-ray-generator energy of 100 keV with copper and tin filters (black and red curves, respectively) are compared with measured spectra (dots).

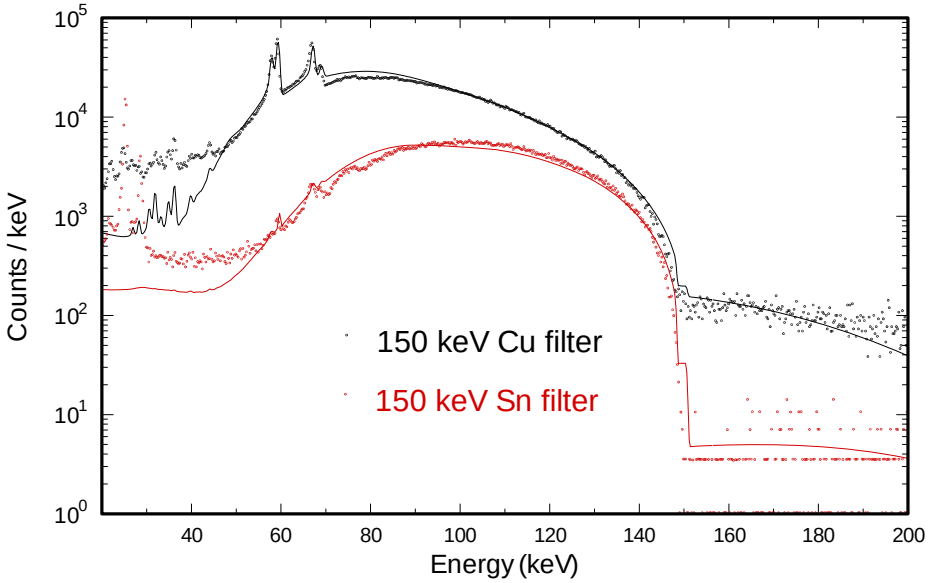

Figure 13. Computed spectra at an x-ray-generator energy of 150 keV with copper and tin filters (black and red curves, respectively) are compared with measured spectra (dots).

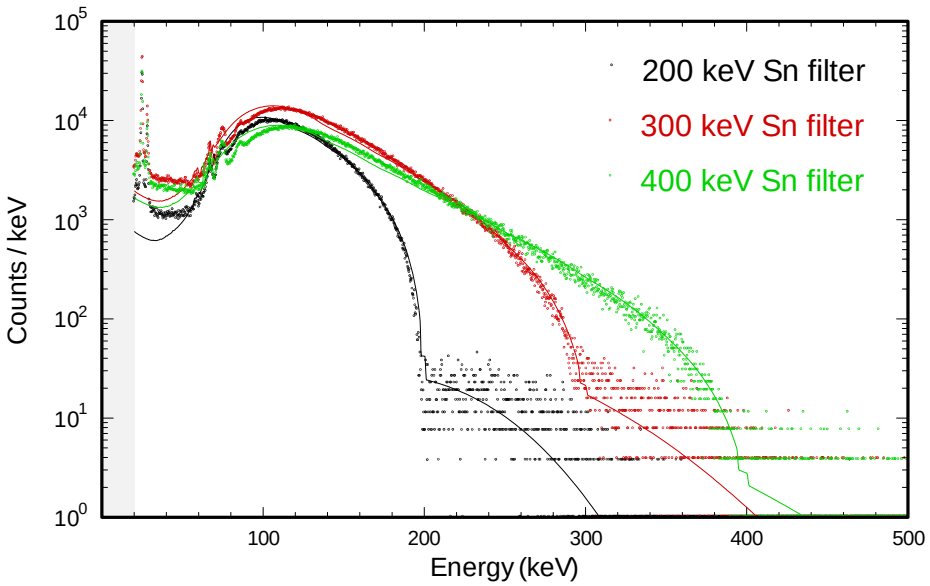

Figure 14. Computed spectra at x-ray-generator energies of 200, 300 and 400 keV with the tin filter (black, red, and green curves, respectively) are compared with measured spectra (dots).

Radiographs are generally processed according to the measured dose as opposed to the electron fluence. The measured dose is a better radiographic metric, particularly in the case of pulsed x-ray generators, because substantial variations in the output are often observed from one pulse to the next. Table 4 compares measured dose rates with calculations based on the interpolated beam profiles. The results are not in complete agreement, but the computed dose rates correlate

reasonably well with measurements. The measured dose was obtained using a Radcal 9010, which reports the Roentgen (R) which is a unit of exposure in air. The conversion from R to absorbed dose (in rad) is 0.95 [2]. The quality factor for gamma rays and x-rays is normally defined to be 1, so that rad and rem are equivalent and the conversion is 0.95 rem/R. The computed dose was derived from ANSI/ANS-6.1.1-1991. However, computed doses differ depending on which standard is selected for the evaluation. Differences in dose values are expected due to non-uniform output of the x-ray system when operated at the minimum current (the system was operated at the minimum tube current values to avoid saturating the x-ray detector).

Table 4. Measured versus computed dose rates as a function of operating voltage.

Operating Voltage	Dose Rate @ 26 cm		
	Measured (R/hr)	Measured (rem/hr)	Computed (rem/hr)
50	16	15	13
60	20	19	17
70	23	22	21
80	25	24	24
90	29	28	28
100	31	29	32
150	43	41	54
200	54	51	76
250	65	62	94
300	71	67	103
350	69	66	102
400	55	52	83

5 Discussion

Measurements that were performed with the small CdTe detector provide an empirical means for evaluating x-ray flux profiles as a function of the x-ray generator voltage. As demonstrated in Section 4, the flux profiles can be adjusted by defining atomic numbers and areal densities for filter materials that are inserted into the beam. However, uncertainties exist due to approximations in the detector response function and the unfolding process that is used to estimate flux profiles. Flux profiles cannot be measured in the same way for pulsed x-ray generators because the excessive pulse pileup would normally occur during the brief periods associated with individual pulses. Although the profiles should be similar regardless of whether a continuous or pulsed x-ray generator is used, they may not be identical. The obvious question is how errors in computed flux profiles impact computed radiographic images.

A previous investigation [3] utilized computed x-ray generator outputs at 8 MeV and 20 MeV [3] as a basis for interpolating the flux profiles at other energies. Extrapolation of the high-energy profiles to the energy range that was characterized in this investigation is a gross approximation, particularly since high-energy and low-energy x-ray generators employ different configurations for the electron beam, the tungsten converter, and the emitted x-ray beam. Therefore,

extrapolations of the high-energy data yield poor representations of the actual profiles. For example, Figure 15 compares the x-ray profiles derived from the two methods with an accelerator voltage of 250 keV and the same integrated dose. The flux profile derived from the current study is dominated by the emission of tungsten x-rays in the 60-keV range whereas extrapolation of the high-energy data yields a featureless continuum.

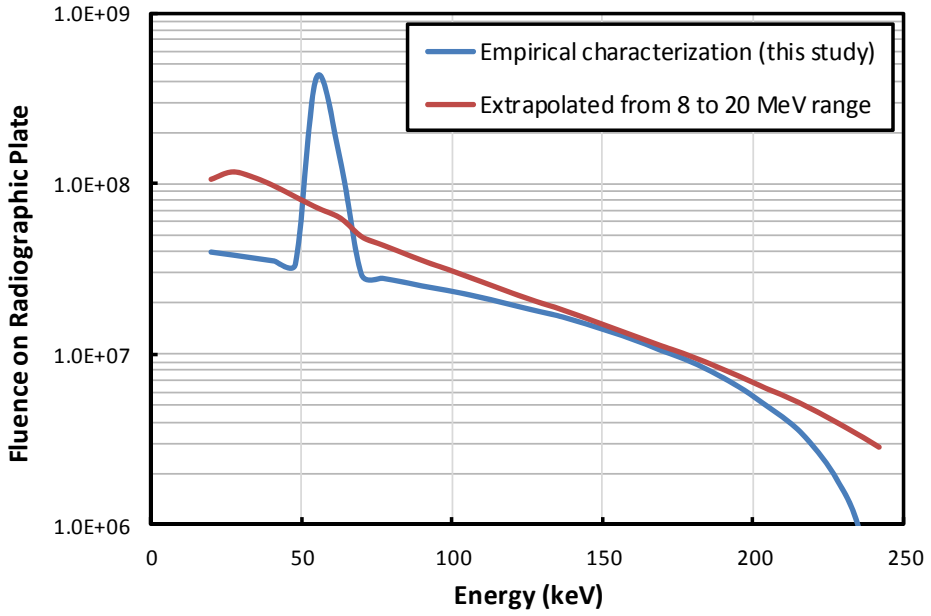

Figure 15. Comparison of estimated x-ray profile derived from this study (blue) at an accelerator voltage of 250 keV with the profile that is obtained by extrapolating the high-energy data.

In order to evaluate the effects associated with the differences in evaluated flux profiles, images were computed based on the two profiles shown in Figure 15. As described in reference [3], these calculations apply a response function to determine the film response to transmitted and scattered radiation. The inspected object used in these simulations was a 2.54 cm radius tungsten ball inside a polyethylene shell with an internal radius of 3 cm and an external radius of 7 cm. The computed images (shown in Figure 16) are visually indistinguishable regardless of which profile is used for the simulation. The same contrast and brightness values were used for the two images, and the unattenuated dose was 50 mrem in both cases. Inspection of the radial profiles provides a more quantitative means for evaluating differences in the calculations. Figure 17 compares the two computed radial profiles with the measured profile for the tungsten ball inside the polyethylene shell. The dose was not recorded in association with the measured image, so the radial profiles were scaled to match the unattenuated pixel value (i.e., the region immediately outside the object). Differences between the two computed radial profiles are small, and they are both in good agreement with the measured radiograph.

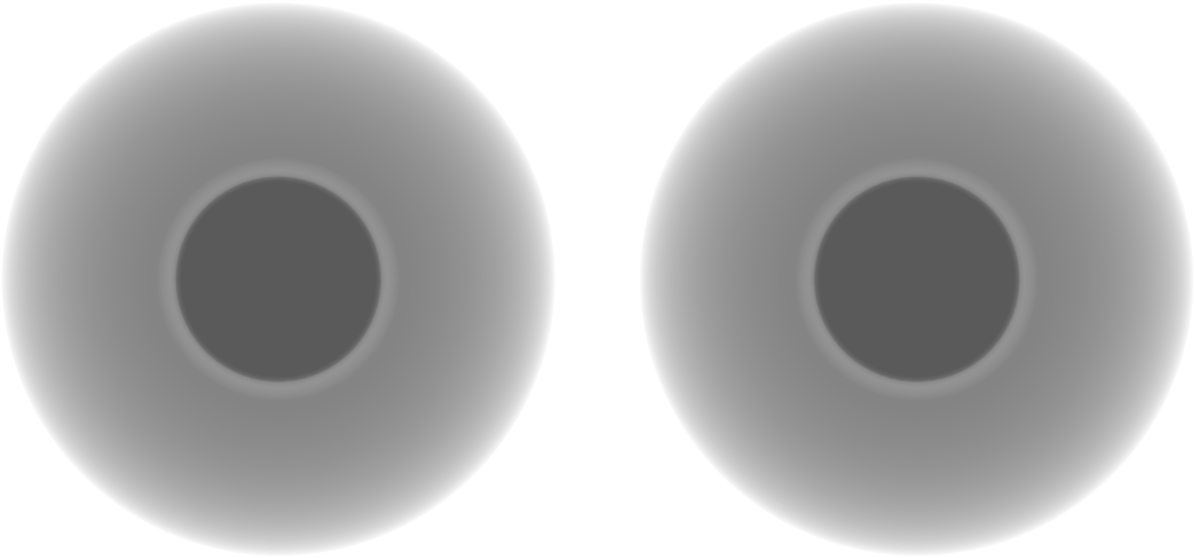

Figure 16. Computed images a tungsten ball inside a polyethylene shell are compared based on the flux profiles shown in Figure 8. The image derived from the flux profile in the current study is on the left and the image derived by extrapolating high-energy data is shown on the right.

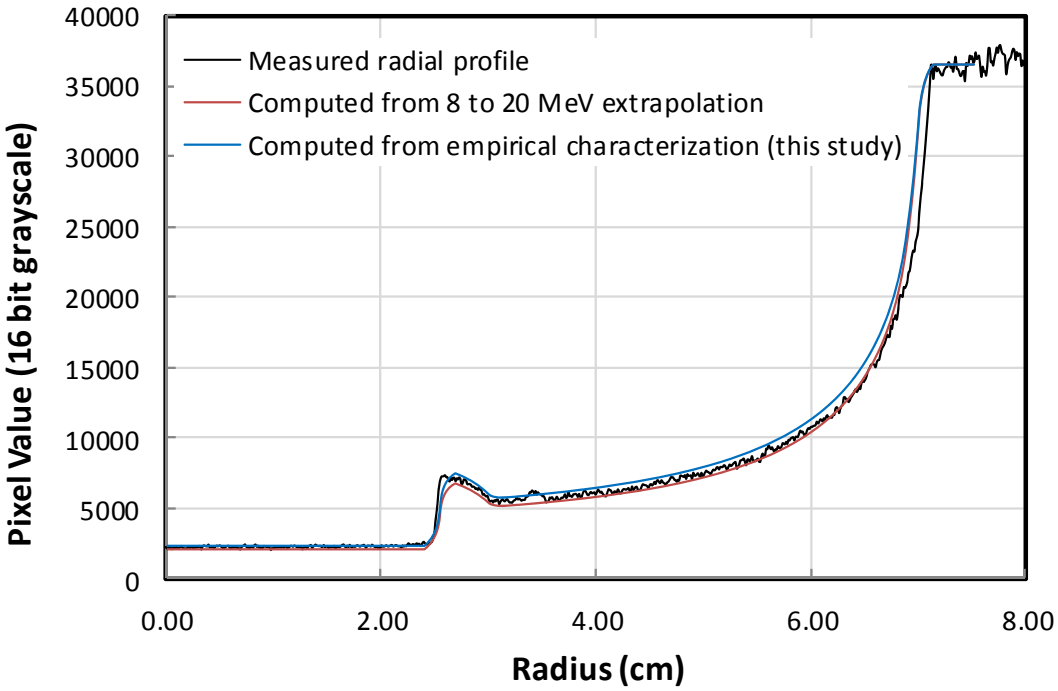

Figure 17. Comparison of computed radial profiles with the measured radial profile for the tungsten ball inside the polyethylene shell.

6 Conclusions

Spectra that were recorded by a small CdTe detector that was placed in front of a continuous x-ray generator were processed to derive flux profiles. The data were reduced to a set of three simple equations that enable computation of beam profiles as a function of the x-ray generator voltage. The accuracy of the derived beam profiles was evaluated by comparing dose measurements with calculations based on the estimated beam profiles over the x-ray generator voltage range 50 keV to 400 keV. The computed dose values agreed with measurements to within 30%. The dose profiles can be adjusted to compensate for filters by defining the atomic number and areal density of the intervening materials. Although the primary effect of filters is to preferentially attenuate low-energy x-rays, the analytic representation of the beam profile also adds scattered radiation. Spectra that are computed with copper and tin filters are in reasonably good agreement with measurements.

Effects associated with differences between beam profile estimates were investigated by computing radiographs based on substantially different evaluations of the beam profile for a 250-keV pulsed x-ray generator. The test object was a small tungsten sphere inside a polyethylene shell. The computed images and radial profiles were very similar despite large differences in the two beam profiles that were used to compute the radiographs. This evaluation suggests that small differences in beam profiles should not have a large impact provided that the calculations are scaled according to either the measured dose or the unattenuated pixel value. Although the results are preliminary, this evaluation also implies that beam profiles measured with a continuous x-ray generator can be applied to pulsed generators.

References

1. Dean J. Mitchell and John Mattingly, “Rapid Computation of Gamma-ray Spectra for One-Dimensional Source Models”, American Nuclear Society: 2008 Annual Meeting (June 2008).

2. James E. Turner, “Atoms, Radiation and Radiation Protection”, Wiley-Interscience (1995).

3. Lee T. Harding, Dean J. Mitchell, and T. Scott Gladwell, “Radiography Simulations for 1-D Models”, Sandia National Laboratories Report SAND2011-7102 (September 2011).

4. James Jones, INL, “Bremsstrahlung Production with Predictive High-Energy Fitting”, private communication (2010).

Distribution

1	MS	0782	Gregory G. Thoreson, 06633
1		0782	Dean J. Mitchell, 06633
1		0782	Lee T. Harding, 06633
1		0782	Mike W. Enghauser, 06633
1		0782	Lisa A. Theisen, 06633
1		0782	George P. Lasche, 06633
1		0782	Charles L. Rhykerd, 06633

1	MS	9018	Central Technical Files, 08523-1
2		0899	Technical Library, 04414